Title

Improving Cosmological Constraints from Galaxy Cluster Number Counts with CMB-cluster-lensing Data: Results from the SPT-SZ Survey and Forecasts for the Future

Authors

Chaubal, PS
Reichardt, CL
Gupta, N
et al.

CrossMark

Improving Cosmological Constraints from Galaxy Cluster Number Counts with CMB-cluster-lensing Data: Results from the SPT-SZ Survey and Forecasts for the Future

P. S. Chaubal[1], C. L. Reichardt[1], N. Gupta[1,2], B. Ansarinejad[1], K. Aylor[3], L. Balkenhol[1], E. J. Baxter[4,5,6], F. Bianchini[7], B. A. Benson[5,6,8], L. E. Bleem[5,9], S. Bocquet[10], J. E. Carlstrom[5,6,9,11,12], C. L. Chang[5,6,9], T. M. Crawford[5,6], A. T. Crites[5,6,13], T. de Haan[14,15], M. A. Dobbs[14,16], W. B. Everett[17], B. Floyd[18], E. M. George[15,19], N. W. Halverson[17,20], W. L. Holzapfel[15], J. D. Hrubes[21], L. Knox[3], A. T. Lee[15,22], D. Luong-Van[21], J. J. McMahon[23], S. S. Meyer[5,6,11,12], L. M. Mocanu[5,6], J. J. Mohr[10,24,25], T. Natoli[5,11,26], S. Padin[5,6], C. Pryke[27], J. E. Ruhl[28], F. Ruppin[29], L. Salvati[30,31,32], A. Saro[30,31,33,34], K. K. Schaffer[5,12,35], E. Shirokoff[5,6,15], Z. Staniszewski[28,36], A. A. Stark[37], J. D. Vieira[38,39], and R. Williamson[5,6]

[1] School of Physics, University of Melbourne, Parkville, VIC 3010, Australia; pchaubal@student.unimelb.edu.au
[2] CSIRO Astronomy and Space Science, P.O. Box 1130, Bentley WA 6102, Australia
[3] Department of Physics, University of California, Davis, CA 95616, USA
[4] Center for Particle Cosmology, Department of Physics and Astronomy, University of Pennsylvania, Philadelphia, PA 19104, USA
[5] Kavli Institute for Cosmological Physics, University of Chicago, Chicago, IL 60637, USA
[6] Department of Astronomy and Astrophysics, University of Chicago, Chicago, IL 60637, USA
[7] Dept. of Physics, Stanford University, 382 Via Pueblo Mall, Stanford, CA 94305, USA
[8] Fermi National Accelerator Laboratory, MS209, P.O. Box 500, Batavia, IL 60510, USA
[9] High Energy Physics Division, Argonne National Laboratory, Argonne, IL 60439, USA
[10] Faculty of Physics, Ludwig-Maximilians-Universität, D-81679 München, Germany
[11] Department of Physics, University of Chicago, Chicago, IL 60637, USA
[12] Enrico Fermi Institute, University of Chicago, Chicago, IL 60637, USA
[13] California Institute of Technology, Pasadena, CA 91125, USA
[14] Department of Physics and McGill Space Institute, McGill University, Montreal, Quebec H3A 2T8, Canada
[15] Department of Physics, University of California, Berkeley, CA 94720, USA
[16] Canadian Institute for Advanced Research, CIFAR Program in Cosmology and Gravity, Toronto, ON, M5G 1Z8, Canada
[17] Center for Astrophysics and Space Astronomy, Department of Astrophysical and Planetary Sciences, University of Colorado, Boulder, CO 80309, USA
[18] Department of Physics and Astronomy, University of Missouri-Kansas City, 5110 Rockhill Road, Kansas City, MO 64110, USA
[19] European Southern Observatory, Karl-Schwarzschild-Straße 2, D-85748 Garching, Germany
[20] Department of Physics, University of Colorado, Boulder, CO 80309, USA
[21] University of Chicago, Chicago, IL 60637, USA
[22] Physics Division, Lawrence Berkeley National Laboratory, Berkeley, CA 94720, USA
[23] Department of Physics, University of Michigan, Ann Arbor, MI 48109, USA
[24] Excellence Cluster Universe, D-85748 Garching, Germany
[25] Max-Planck-Institut für extraterrestrische Physik, D-85748 Garching, Germany
[26] Dunlap Institute for Astronomy & Astrophysics, University of Toronto, 50 St George St, Toronto, ON, M5S 3H4, Canada
[27] Department of Physics, University of Minnesota, Minneapolis, MN 55455, USA
[28] Physics Department, Center for Education and Research in Cosmology and Astrophysics, Case Western Reserve University, Cleveland, OH 44106, USA
[29] Kavli Institute for Astrophysics and Space Research, Massachusetts Institute of Technology, 77 Massachusetts Avenue, Cambridge, MA 02139, USA
[30] INAF-Osservatorio Astronomico di Trieste, via G.B. Tiepolo 11, I-34143 Trieste, Italy
[31] IFPU—Institute for Fundamental Physics of the Universe, via Beirut 2, I-34014 Trieste, Italy
[32] Universite Paris-Saclay, CNRS, Institut d'strophysique Spatiale, F-91405, Orsay, France
[33] Astronomy Unit, Department of Physics, University of Trieste, via Tiepolo 11, I-3413 Trieste, Italy
[34] INFN-Sezione di Trieste, Trieste, Italy
[35] Liberal Arts Department, School of the Art Institute of Chicago, Chicago, IL 60603, USA
[36] Jet Propulsion Laboratory, California Institute of Technology, Pasadena, CA 91109, USA
[37] Harvard-Smithsonian Center for Astrophysics, Cambridge, MA 02138, USA
[38] Astronomy Department, University of Illinois at Urbana-Champaign, 1002 W. Green Street, Urbana, IL 61801, USA
[39] Department of Physics, University of Illinois Urbana-Champaign, 1110 W. Green Street, Urbana, IL 61801, USA

Abstract

We show the improvement to cosmological constraints from galaxy cluster surveys with the addition of cosmic microwave background (CMB)-cluster lensing data. We explore the cosmological implications of adding mass information from the 3.1σ detection of gravitational lensing of the CMB by galaxy clusters to the Sunyaev–Zel'dovich (SZ) selected galaxy cluster sample from the 2500 deg^2 SPT-SZ survey and targeted optical and X-ray follow-up data. In the ΛCDM model, the combination of the cluster sample with the Planck power spectrum measurements prefers $\sigma_8(\Omega_m/0.3)^{0.5} = 0.831 \pm 0.020$. Adding the cluster data reduces the uncertainty on this quantity by a factor of 1.4, which is unchanged whether the 3.1σ CMB-cluster lensing measurement is included or not. We then forecast the impact of CMB-cluster lensing measurements with future cluster catalogs. Adding CMB-cluster lensing measurements to the SZ cluster catalog of the ongoing SPT-3G survey is expected to improve the

expected constraint on the dark energy equation of state w by a factor of 1.3 to $\sigma(w) = 0.19$. We find the largest improvements from CMB-cluster lensing measurements to be for σ_8, where adding CMB-cluster lensing data to the cluster number counts reduces the expected uncertainty on σ_8 by respective factors of 2.4 and 3.6 for SPT-3G and CMB-S4.

Unified Astronomy Thesaurus concepts: Cosmology (343); Sigma8 (1455)

1. Introduction

Galaxy clusters are the largest gravitationally collapsed structures and a key testing ground of cosmological models of structure growth (Allen et al. 2011). The number density of galaxy clusters depends sensitively upon cosmological parameters, in particular those that affect late-time structure growth, such as the sum of the neutrino masses, the dark energy equation of state, and matter density (Wang & Steinhardt 1998; Haiman et al. 2001; Weller et al. 2002; Weller & Battye 2003; Holder 2006; Shimon et al. 2011). Upcoming surveys such as eROSITA (Merloni et al. 2012), LSST (LSST Science Collaboration et al. 2009; The LSST Dark Energy Science Collaboration et al 2018), and CMB-S4 (CMB-S4 Collaboration 2019) are expected to detect tens of thousands of galaxy clusters at different wavelengths, and will dramatically improve the cosmological constraints from cluster cosmology.

Galaxy clusters have already yield interesting constraints on the matter density Ω_m and the amplitude of density fluctuations σ_8 (Bocquet et al. 2019; Zubeldia & Challinor 2019; To et al. 2021). The cosmological constraints are limited, however, by the uncertainty on the masses of galaxy clusters, and they can be biased if the cluster mass-observable scaling relations are misestimated. Current cluster mass estimates are typically based on assuming a power-law scaling relationship between observed quantities (such as the X-ray observable Y_X) and cluster masses. Observationally expensive optical weak-lensing measurements are used to normalize the scaling relation (e.g., Dietrich et al. 2019). These optical weak-lensing mass measurements should substantially improve with surveys like LSST and Euclid (The LSST Dark Energy Science Collaboration et al 2018; Euclid Collaboration et al. 2019). At higher redshifts ($z \gtrsim 1$), optical weak lensing becomes increasingly difficult due to a dearth of background galaxies and the difficulties in measuring their shape with blending and lower signal-to-noise ratios (S/N). High-redshift mass information is important because there are suggestions that scaling relations calibrated at lower redshifts may misestimate the masses at higher redshifts (Salvati et al. 2018, 2019; Zohren et al. 2019).

Galaxy clusters also gravitationally lens the cosmic microwave background (CMB), an effect referred to as CMB-cluster lensing and first considered by Seljak & Zaldarriaga (2000). While useful as an independent cross-check on optical weak-lensing cluster masses at low redshift, CMB-cluster lensing is particularly useful at higher redshifts. Since all CMB photons originate at the same extremely high redshift, $z \simeq 1100$, the S/N of CMB-cluster lensing does not drop as the cluster redshift increases (Melin & Bartlett 2015). This also simplifies the measurement (and eliminates related uncertainties), as one does not need to calculate intrinsic alignments, boost factors, or the redshift distribution to background sources. The problem of estimating the masses of clusters from their CMB lensing signals has been extensively considered (Seljak & Zaldarriaga 2000; Dodelson 2004; Holder & Kosowsky 2004; Vale & Ostriker 2004; Lewis & Challinor 2006; Lewis & King 2006; Hu et al. 2007; Raghunathan et al. 2017, 2019a;

Gupta & Reichardt 2021). Actual measurements of the CMB-cluster lensing signal have followed as CMB surveys have advanced, from the first detections in 2015 (Baxter et al. 2015; Madhavacheril et al. 2015; Planck Collaboration et al. 2016) to ~15% mass measurements of different cluster samples today (Baxter et al. 2018; Raghunathan et al. 2019b).

In this work, we present the first cosmological analysis of the SPT-SZ galaxy cluster sample that includes CMB-cluster lensing information. The SPT-SZ survey detected galaxy clusters from the imprint of thermal SZ (tSZ) signatures on the background primary CMB anisotropies (Bleem et al. 2015). Bocquet et al. (2019, hereafter B19) presented cosmological constraints from this sample along with X-ray observations and optical weak-lensing measurements. We add the CMB-cluster lensing mass measurement of Baxter et al. (2015, hereafter B15) to that data set, and look at the implications for the combined data set on the ΛCDM and wCDM cosmological models. We follow this by presenting forecasts for the cosmological constraints from future CMB-cluster lensing measurements with SPT-3G (Benson et al. 2014) and CMB-S4 (CMB-S4 Collaboration 2019). We do not explore CMB-cluster lensing systematics in this work, as these have already been extensively discussed (Raghunathan et al. 2017; Baxter et al. 2018; Zubeldia & Challinor 2020). We find that CMB-cluster lensing mass measurements substantially improve the predicted constraints on the dark energy equation of state parameter w from future cluster catalogs.

The paper is organized as follows. In Section 2, we review the data sets used in this analysis. We describe the analysis methods in Section 3. In Section 4, we present the cosmological constraints from the current CMB-cluster lensing measurement. In Section 5, we forecast the constraints expected from the ongoing SPT-3G and future CMB-S4 surveys. Finally, we conclude in Section 6. Throughout this work, we report galaxy cluster masses in terms of either M_{200} or M_{500}, the mass contained within the radius where the mean density is 200 (500) times the critical density of the universe.

2. The Cluster Catalog from the 2500d SPT-SZ Survey

The main data set in this work is the galaxy cluster sample from the 2500d SPT-SZ survey (Bleem et al. 2015), which provides a measure of the SZ detection significance and redshift for each cluster in the sample. As in the previous cosmological analysis by B19, we supplement the SZ cluster catalog with follow-up X-ray and optical weak-lensing observations. The new addition in this work is that we add the 3.1σ CMB-cluster lensing mass measurement from B15 for a stack of 513 of galaxy clusters in the sample. This subsample of 513 clusters is chosen by selecting only those clusters from the 2500d SPT-SZ catalog that have measured optical redshifts. We refer to the combination of SPT number counts, X-ray and weak-lensing follow-up, and CMB-cluster lensing data sets as SPT clusters. We briefly describe these data sets in the following subsections.

For some parameter fits, we also include measurements of the CMB TT, TE, and EE power spectra from the 2018 data release of the Planck satellite (Planck Collaboration et al. 2020). We refer to this data set as "Planck" throughout rest of the work. The Planck CMB data allow us to demonstrate where clusters and CMB-cluster lensing add the most information.

2.1. SZ Detection Significance and Cluster Redshift

The SZ detection significance and cluster redshift (or lower limit on redshift) are reported for all cluster candidates in the Bleem et al. (2015) catalog and were later updated in B19. The reported significance is the maximum across a set of matched filters (to allow for variations in the cluster angular radius with redshift and mass), and therefore is biased high on average. To avoid this biasing in the mass estimates, we follow B19 in using the unbiased significance $\zeta = \sqrt{(\xi^2 - 3)}$ as a mass proxy. A detailed discussion on the validity of this approach can be found in Vanderlinde et al. (2010). As in B19, we model the relationship between the unbiased significance ζ and cluster mass M_{500} as:

$$\zeta = A_{\rm SZ}\left(\frac{M_{500}h_{70}}{4.3 \times 10^{14}M_\odot}\right)^{B_{\rm SZ}}\left(\frac{E(z)}{E(0.6)}\right)^{C_{\rm SZ}}, \qquad (1)$$

where $A_{\rm SZ}$, $B_{\rm SZ}$, and $C_{\rm SZ}$ are free parameters in the model fits (see Table 1) and $E(z)$ is the dimensionless Hubble parameter. Here, h_{70} is the Hubble constant divided by 70 km s^{-1} Mpc^{-1}, and z is the cluster redshift. The intrinsic scatter in $\ln\zeta$ at a fixed mass and redshift is modeled as a Gaussian scatter with width $\sigma_{\ln\zeta}$, and is also left as a free parameter of the model.

2.2. Weak-lensing Shear Profiles

Thirty-two clusters have optical weak-lensing shear profiles, with 13 from the Hubble Space Telescope and 19 from ground-based Megacam/Magellan imaging (Schrabback et al. 2018; Dietrich et al. 2019). The shear profiles of these clusters are compared to the expected weak-lensing shear profiles under the assumption of a Navarro–Frenk–White profile (Navarro et al. 1997) for the cluster density. We allow for a systematic bias $b_{\rm WL}$ between the halo mass $M_{\rm halo}$ and inferred lensing mass $M_{\rm WL}$:

$$M_{\rm WL} = b_{\rm WL}M_{\rm halo}. \qquad (2)$$

We refer the reader to Equation (9) in B19 for the breakdown of $b_{\rm WL}$ into different sources of uncertainty in the weak-lensing observations. The priors on these uncertainties are included in Table 1 under the *WL modeling* section. The weak-lensing model is described in more detail by B19.

2.3. X-Ray Y_X Data

As in B19, we use X-ray observations of 89 galaxy clusters taken through a Chandra X-ray visionary project (McDonald et al. 2013, 2017). The X-ray data are used to estimate Y_X (the product of the gas mass and X-ray temperature) within r_{500} for each cluster. We assume a scaling relation between Y_X and the

Table 1
Parameter Priors

Parameter	Prior
SZ scaling relation	
$A_{\rm SZ}$	$\mathcal{U}(1, 10)$
$B_{\rm SZ}$	$\mathcal{U}(1, 2.0)$
$C_{\rm SZ}$	$\mathcal{U}(-1, 2)$
$\sigma_{\ln\zeta}$	$\mathcal{U}(0.01, 2.0)$
Priors for the SPT-SZ cluster catalog	
X-ray Y_X scaling relation	
A_{Y_X}	$\mathcal{U}(3, 10)$
B_{Y_X}	$\mathcal{U}(0.3, 0.9)$
C_{Y_X}	$\mathcal{U}(-1, 0.5)$
$\sigma_{\ln Y_X}$	$\mathcal{U}(0.01, 0.5)$
$d\ln M_{\rm g}/d\ln r$	$\mathcal{N}(1.12, 0.23^2)$
WL modeling	
$\delta_{\rm WL,bias}$	$\mathcal{N}(0, 1)$
$\delta_{\rm Megacam}$	$\mathcal{N}(0, 1)$
$\delta_{\rm HST}$	$\mathcal{N}(0, 1)$
$\delta_{\rm WL,scatter}$	$\mathcal{N}(0, 1)$
$\delta_{\rm WL,LSS_{Megacam}}$	$\mathcal{N}(0, 1)$
$\delta_{\rm WL,LSS_{HST}}$	$\mathcal{N}(0, 1)$
Correlated scatter	
$\rho_{\rm SZ\text{-}WL}$	$\mathcal{U}(-1, 1)$
$\rho_{\rm SZ\text{-}X}$	$\mathcal{U}(-1, 1)$
$\rho_{\rm X\text{-}WL}$	$\mathcal{U}(-1, 1)$
	$\det(\Sigma_{\rm multi\text{-}obs}) > 0$
Priors on cluster-only chains	
$\Omega_b h^2$	$\mathcal{N}(0.02212, 0.00022^2)$
τ	$\mathcal{N}(0.0522, 0.0080^2)$
$10^9 A_s$	$\mathcal{N}(2.092, 0.033^2)$
n_s	$\mathcal{N}(0.9626, 0.0057^2)$

Note. The parameter priors used in this analysis are listed here. The symbol $\mathcal{U}$ denotes a uniform prior over the given range while $\mathcal{N}(\mu, \sigma^2)$ denotes a Gaussian prior centered at μ with variance σ^2. The SZ scaling relation priors are used for all results in this work that include cluster data, while the cluster-only priors listed in the bottom section are only used in cluster-only MCMCs. The priors in the X-ray, WL modeling, and Correlated scatter section are used for the SPT-SZ cluster data, but not in forecasts for future experiments.

cluster mass M_{500} of the form:

$$\ln\left(\frac{M_{500}h_{70}}{8.37 \times 10^{13}M_\odot}\right) = \ln A_{Y_X} + B_{Y_X}\langle\ln Y_X\rangle$$
$$+ B_{Y_X}\ln\left(\frac{h_{70}^{5/2}}{3 \times 10^{14}M_\odot{\rm keV}}\right)$$
$$+ C_{Y_X}\ln E(z). \qquad (3)$$

The intrinsic scatter in $\ln Y_X$ at fixed mass and redshift is modeled as a normal distribution with width $\sigma_{\ln Y_X}$.

2.4. CMB-cluster Lensing Measurement

CMB photons are deflected by the gravitational pull of galaxy clusters. This deflection remaps the CMB anisotropy, and introduces a dipole-like signal aligned with the local gradient in the primary CMB anisotropy (Lewis & Challinor 2006). B15 extracted this CMB-cluster lensing signal from the SPT-SZ survey data at the positions of clusters in the

SPT-SZ sample. To avoid being biased by the cluster's own tSZ signal, B15 used a linear combination of the 90, 150, and 220 GHz maps from the SPT-SZ survey to make a tSZ-free map for the analysis. We refer the reader to B15 for further details on the measurement.

For the SPT-SZ catalog subsample described in Section 2, B15 found the mean mass of the stacked clusters to be $\bar{M}_{200} = (5.1 \pm 2.1) \times 10^{14} M_\odot$. We convert M_{200} to M_{500} by assuming a concentration parameter $c = 3$ and the same flat ΛCDM cosmological parameters used in B15 ($\Omega_m = 0.3$, $h = 0.7$) for the redshift of $z = 0.7$. This gives us a value of $M_{500} = (3.49 \pm 0.74) \times 10^{14} M_\odot$, which we use in our analysis. We note that converting the mean mass of the stack from M_{200} to M_{500} is not equivalent to converting individual cluster masses before stacking, as the concentration–mass relation is redshift-dependent. For this sample, this approximation results in a $\sim$2% systematic error, which is negligible at the current statistical uncertainty, although the approximation may be inadequate for future high-S/N mass measurements.

3. Likelihood

As in past SPT-SZ cluster analyses (Reichardt et al. 2013; de Haan et al. 2016; Bocquet et al. 2019), we derive cosmological constraints from galaxy clusters by using the Cash statistic (Cash 1979) to compare the expected number of clusters with the observed number as a function of the SZ signal and redshift. The number density of clusters is predicted from the matter power spectrum and mass-observable scaling relations for each set of model parameters. Here, we briefly review the likelihood,[40] which is presented in more detail by B19, before describing how we incorporate the new CMB-cluster lensing information.

We choose to express the likelihood function in three parts: cluster abundances ($\mathcal{L}_{abund}$), mass calibration from the weak-lensing and X-ray observations ($\mathcal{L}_{fol}$), and mass calibration from the CMB-cluster lensing observation ($\mathcal{L}_{CL}$). The abundance part (which is unchanged from B19) calculates the chance of finding a catalog of clusters with the specified redshifts and SZ significances as a function of the cosmology and scaling relations. As in B19, the X-ray and weak-lensing mass calibration likelihood is expressed as:

$$
\begin{aligned}
\mathcal{L}_{fol} \equiv\ & P(Y_X^{obs}, g_t^{obs}|\xi, z, \boldsymbol{p}) \\
=\ & \iint \iint dM\, d\zeta\, dY_X dM_{WL} \\
& \times [P(Y_X^{obs}|Y_X)P(g_t^{obs}|M_{WL})P(\xi|\zeta) \\
& \times P(\zeta, Y_X, M_{WL}|M, z, \boldsymbol{p})P(M|z, \boldsymbol{p})].
\end{aligned}
\tag{4}
$$

This equation gives the likelihood of observing the follow-up X-ray, Y_X^{obs}, and weak-lensing, g_t^{obs}, observables for a cluster detected with SZ significance ξ. Here, $\boldsymbol{p}$ represents cosmological and scaling relation parameters. We assume the systematics in the CMB-cluster lensing measurement to be uncorrelated with other observations. The notation adopted for other variables is identical to that of B19.

While we could exactly mirror the approach used for including weak-lensing data, the CMB-cluster lensing signal from individual clusters is too weak to justify the computational complexity. Instead, we take the observed mean mass

from CMB-cluster lensing $\bar{M}_{200} = (5.1 \pm 2.1) \times 10^{14} M_\odot$ as a prior on the modeled mean mass of the sample, $\bar{M}$:

$$
\bar{M} = \frac{1}{N} \sum_i \iint d\xi_i dz_i\, M_i P(M_i|\xi_i, z_i) P(\xi_i, z_i|\boldsymbol{p}).
\tag{5}
$$

Given the number of clusters in the sample, we approximate the integral by taking the mass at the peak of the posterior for each cluster in the sample.

4. Parameter Constraints

We now turn to the cosmological implications of the CMB-cluster lensing measurement and cluster catalog described in Section 2 using the likelihood function described in Section 3. All MCMC analyses use the same priors for the scaling relations, which are listed in Table 1.

We infer cosmological constraints using the publicly available COSMOSIS parameter estimation code (Zuntz et al. 2015), running the Boltzmann code package CAMB (Lewis et al. 2000). We use the *Multinest* or *emcee* samplers (Feroz et al. 2009; Foreman-Mackey et al. 2013) as implemented by COSMOSIS. Multinest is run with 250 live points with a tolerance value of 0.1. We look at two cosmological models: the standard six-parameter ΛCDM model with fixed $\sum m_\nu = 0.06$ eV, and a well-motivated extension to ΛCDM where the dark energy equation of state, w, is allowed to vary.

4.1. ΛCDM Cosmology

Galaxy cluster number counts are very sensitive to the growth of matter perturbations. Previous works have found galaxy clusters to best constrain the parameters combination $S_8 = \sigma_8(\Omega_m/0.3)^{0.5}$. For the SPT cluster sample with Planck power spectrum measurement, we find:

$$
S_8 = 0.831 \pm 0.020.
\tag{6}
$$

The uncertainty is larger than Planck-only by a factor of 1.4 , due to the tension between the Planck data favoring $S_8 = 0.834 \pm 0.016$ and cluster data favoring a lower $S_8 = 0.794 \pm 0.049$. The result is similar to what was found in B19, so we do not attribute it to CMB-cluster lensing. The similarity is understandable because the S/N on the CMB-cluster lensing is low compared to optical weak lensing. For instance, changing the mass normalization A_{SZ} from 4.4 to 5.5, the weak-lensing log-likelihood changes by $\Delta \ln \mathcal{L}_{WL} = -5.8$, 15 times greater than the change in the CMB-cluster lensing log-likelihood of $\Delta \ln \mathcal{L}_{CMBcl} = -0.38$ for the same shift. As noted above for S_8, the modest tension between the cluster and Planck data leads to slightly wider constraints for the combined data set on Ω_m and σ_8:

$$
\Omega_m = 0.316 \pm 0.011,
\tag{7}
$$

$$
\sigma_8 = 0.8081 \pm 0.0079.
\tag{8}
$$

We report the parameter constraints on selected cosmological and scaling relation parameters obtained from either the SPT clusters or Planck data sets in Table 2.

4.2. wCDM

Clusters are an important probe of the late-time universe when dark energy dominates the energy budget. We therefore consider the impact of the cluster abundance and CMB-cluster lensing measurement on the dark energy equation of state

---

[40] https://github.com/SebastianBocquet/SPT_SZ_cluster_likelihood

Table 2
Parameter Constraints for the Planck and SPT-SZ Surveys

Parameter	ΛCDM		wCDM	
	Planck	SPT Clusters	Planck	SPT Clusters
Ω_m	0.3165 ± 0.0084	0.352 ± 0.047	0.184 ± 0.045	0.279 ± 0.042
σ_8	0.8118 ± 0.0072	0.737 ± 0.033	0.985 ± 0.077	0.772 ± 0.037
S_8	0.834 ± 0.016	0.794 ± 0.049	0.774 ± 0.031	0.743 ± 0.048
w	⋯	⋯	-1.63 ± 0.28	-1.07 ± 0.20
A_{SZ}	⋯	5.3 ± 1.1	⋯	5.1 ± 1.2
B_{SZ}	⋯	1.668 ± 0.068	⋯	1.631 ± 0.068
C_{SZ}	⋯	1.09 ± 0.30	⋯	0.73 ± 0.24
$\sigma_{\ln \zeta}$	⋯	0.168 ± 0.076	⋯	0.176 ± 0.071

Note. Summary of constraints obtained from the cluster data for the ΛCDM and wCDM cosmological models. We obtain the constraints under the SPT Clusters column from the SPT-SZ cluster data set without including the Planck data set. Constraints obtained from using the Planck data set are given for comparison.

parameter w. The cluster data favor

$$w = -1.07 \pm 0.20, \qquad (9)$$

consistent with a cosmological constant. As shown in Figure 1, the cluster abundance data prefer a higher value of the dark energy equation of state as the matter density increases. The detection significance of the B15 CMB-cluster lensing measurement is as yet too low to significantly tighten the allowed parameter volume. While this uncertainty on w is modestly tighter than that inferred from Planck power spectra alone ($w = -1.56^{+0.19}_{-0.39}$), combining the cluster abundance and Planck CMB data significantly reduces the allowed region to:

$$w = -1.30 \pm 0.10. \qquad (10)$$

5. Forecasts

We now examine the expected impact of CMB-cluster lensing on the cosmological constraints from upcoming galaxy cluster surveys. Using the likelihood framework from Section 3, we forecast the results from two surveys: the ongoing SPT-3G survey, and the planned CMB-S4 survey. We assume that SPT-3G will survey 1500 deg² with a temperature map noise level of 2.5 μK-arcmin (polarization map noise level a factor of $\sqrt{2}$ higher) at 150 GHz (Sobrin et al. 2022) and produce a catalog of ∼3600 clusters above an S/N of 4.5. After galactic cuts, we assume the CMB-S4 survey will cover 60% of the sky with a map noise level of 1.0 μK-arcmin (polarization map noise level a factor of $\sqrt{2}$ higher) at 150 GHz (CMB-S4 Collaboration 2019) and produce a catalog of ∼135,000 clusters above an S/N of 4.5. CMB-S4 will survey 3% of the sky to even lower noise levels, and thus is expected to add a further 17,000 clusters. Catalogs from both CMB-S4 surveys are used in the forecasts in this work. We look at the results for the cluster abundances alone and in combination with mass information from optical weak lensing or CMB-cluster lensing. The redshift bins and the uncertainties for SPT-3G and CMB-S4 surveys are described below.

For the full SPT-3G survey, we expect CMB-cluster lensing to lead to a 4.6% mass measurement across the entire cluster sample (Raghunathan et al. 2017). Given the high detection significance, we choose to subdivide the cluster catalog into four redshift bins to better constrain any redshift evolution in the relationship between SZ flux and mass. The four redshift bins are [0.25, 0.55), [0.55,0.78), [0.78, 1.06), and [1.06, 2.0],

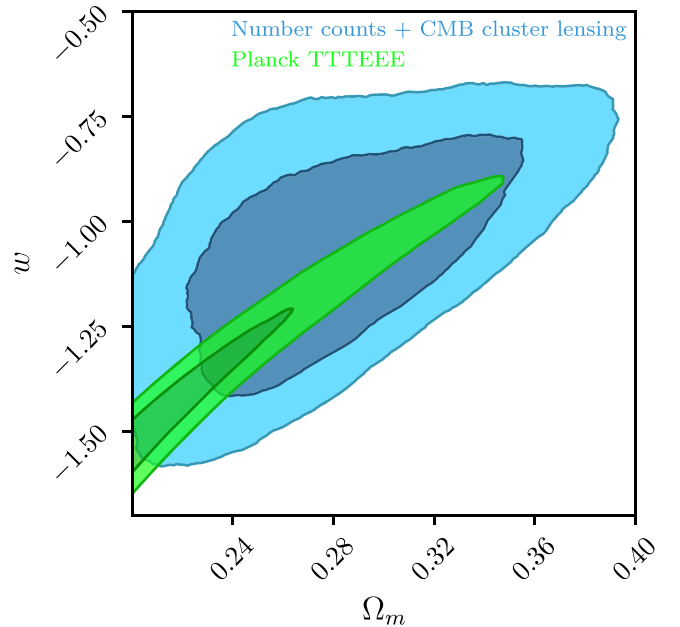**Figure 1.** Constraints on Ω_m and w in the wCDM model from the SPT-SZ cluster data set (blue contours) and the Planck TTTEEE power spectra (green contours). The SPT-SZ cluster count constraints are obtained using CMB-cluster lensing information along with information from follow-up data sets. The cluster data help break the degeneracy between Ω_m and w that exists in the CMB power spectra alone.

allowing us to achieve a roughly equal number of clusters and lensing detection significance in each bin. The uncertainty on the average mass of the clusters in each of the four bins is taken to be 9.2%. For simplicity, we assume equal constraining power in each of the bins. We do not include the effect of systematic uncertainties, such as from tSZ contamination or errors in the assumed mass profile, but we direct interested readers toward Raghunathan et al. (2017) for a discussion of potential systematic errors and their magnitude. The potential systematic biases are expected to be correctable to better than the mass uncertainties assumed in this work. We conservatively assume a 5% mass calibration from optical weak lensing at $z < 0.8$, again implemented as four 10% mass constraints on redshift bins running [0.25, 0.39), [0.39, 0.53), [0.53, 0.67), and [0.67, 0.8], such as might be achieved from the final DES results (McClintock et al. 2019).

The CMB-S4 survey is expected to start in the second half of this decade. As such, we assume substantially improved optical
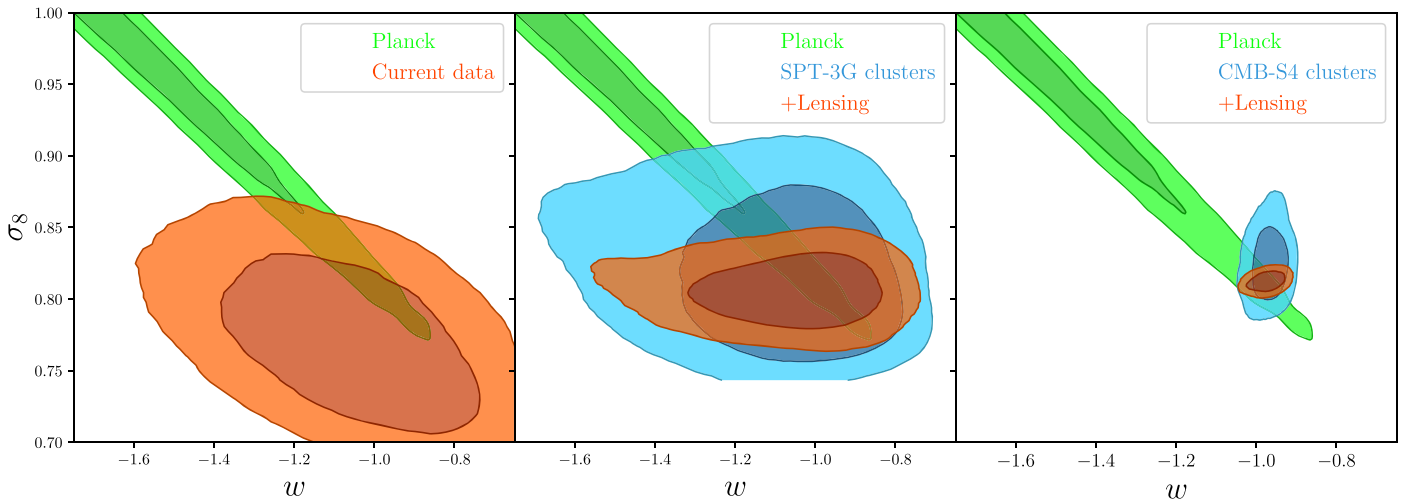
Figure 2. The 1σ and 2σ contours for σ_8 and w in the wCDM model for the SPT-SZ (left panel), SPT-3G (middle panel), and CMB-S4 (right panel) surveys. The SPT-3G and CMB-S4 contours are forecasts from simulated cluster catalogs created for $\sigma_8 = 0.8126$ and $w = -1$. Parameter posterior distributions from the Planck CMB data are shown in green, while the posteriors from cluster number counts are shown in blue. The posterior distributions from cluster number counts and CMB-cluster lensing are shown in orange. Adding CMB-cluster lensing information significantly improves the constraints on equation of dark energy parameter w and σ_8.

Table 3
Forecasts for Parameter Constraints for Upcoming Surveys

Survey	Data	Ω_m	h	w	σ_8	S_8
Planck	CMB TTTEEE power spectra	0.045	0.10	0.28	0.077	0.031
SPT-3G	Number counts	0.026	0.030	0.19	0.039	0.051
	+ CMB-cluster lensing	0.025	0.028	0.15	0.016	0.025
	+ CMB-cluster and optical weak lensing	0.024	0.024	0.14	0.014	0.023
CMB-S4	Number counts	0.0063	0.012	0.028	0.016	0.016
	+ CMB-cluster lensing	0.0057	0.0092	0.029	0.0044	0.0059
	+ CMB-cluster and 2% optical weak lensing	0.0052	0.0071	0.023	0.0040	0.0059
	+ CMB-cluster and 1% optical weak lensing	0.0050	0.0072	0.020	0.0046	0.0059

Note. Cluster counts from SPT-3G and CMB-S4 can significantly improve cosmological constraints. We report here forecasted constraints in the seven-parameter wCDM model for w, σ_8, and $S_8 \equiv \sigma_8\sqrt{\Omega_m/0.3}$. The second row has current uncertainties from the Planck 2018 TTTEEE data, shown for comparison. The third through fifth rows have, in order, the expected uncertainties with the SPT-3G cluster counts, with the SPT-3G cluster counts and CMB-cluster lensing mass measurement, with the SPT-3G cluster counts and a DES-like optical weak-lensing mass measurement, and with both the optical and CMB-cluster lensing mass measurements. The sixth through ninth rows are the same except for CMB-S4 and two options for an LSST-like optical survey that yields either a 1% or 2% mass measurement. Adding the optical weak-lensing mass measurements to the CMB-S4 catalog does not improve estimates of large-scale structure today (i.e., σ_8), but it does noticeably improve the constraints on the dark energy equation of state.

weak-lensing mass measurements will be available from, for instance, LSST or Euclid, and provide either a 2% (conservative) or 1% (goal) mass calibration (Grandis et al. 2019). As before, we implement this as either a 4% or 2% mass calibration in each of four redshift bins that cover the redshift range from $z = 0.25$ to 0.8. The lower-noise CMB maps will also enable tighter mass constraints from CMB-cluster lensing. From Raghunathan et al. (2017), we estimate that the CMB-S4 wide survey will yield a 3% mass calibration in each of the four redshift bins, while the deep survey will yield a 5% mass calibration that is weaker (due to fewer clusters) in each redshift bin. As with SPT-3G, we do not include the effect of systematic errors.

As shown in Table 3 and Figure 2, we find that adding the mass information from optical weak lensing and CMB-cluster lensing substantially improves cosmological constraints from galaxy cluster abundances with SPT-3G and CMB-S4. Assuming that that posteriors are approximately Gaussian, we calculate the allowed parameter volume as the square root of the determinant of the covariance matrix. The allowed parameter

volume from the cluster abundance data for the seven parameters of the wCDM model is reduced by a factor of 4.1 for SPT-3G and 6.1 for CMB-S4, by adding the CMB-cluster and optical lensing measurements. While the absolute mass calibration is similar between the optical and CMB lensing channels ($\sim$5% for SPT-3G and $\sim$2%–3% for CMB-S4), the higher-redshift lever arm in the CMB-cluster lensing measurement has advantages for the SZ cluster catalogs, with their high median redshifts ($\sim$0.8 for both the SPT-3G and CMB-S4 surveys). For the SPT-3G cluster sample, adding only the CMB-cluster lensing measurement reduces the parameter volume by a factor of 2.8. Adding both CMB-cluster lensing and optical weak lensing improves the parameter volume by a factor of 4.1, as stated above. This translates to an improvement on w from $\sigma(w) = 0.19$ for cluster counts to $\sigma(w) = 0.15$ with CMB-cluster lensing and $\sigma(w) = 0.14$ with CMB-cluster lensing and optical weak-lensing information (the latter two uncertainties are consistent, given the number of samples in the MCMC). The expected constraint on σ_8 shows an even larger improvement, tightening from $\sigma(\sigma_8) = 0.039$ for cluster counts to $\sigma(\sigma_8) = 0.016$ with

CMB-cluster lensing and $\sigma(\sigma_8) = 0.014$ with CMB-cluster lensing and optical weak-lensing information. The story is similar for CMB-S4. The seven-parameter volume is reduced by a factor of 4.8 (6.1) by adding CMB-cluster lensing (both CMB-cluster lensing and a 2% optical weak-lensing measurement). Adding both the optical weak-lensing and CMB-cluster lensing information brings $\sigma(w) = 0.028$ down to $\sigma(w) = 0.023$ for a 2% mass calibration ($\sigma(w) = 0.020$ for a 1% mass calibration), a factor of 1.2 (1.4) improvement over the cluster counts alone. The CMB-cluster lensing information substantially improves the constraint on σ_8 from the CMB-S4 cluster catalog by more than a factor of three, from $\sigma(\sigma_8) = 0.016$ to $\sigma(\sigma_8) = 0.0044$. Adding a 1% (2%) optical weak-lensing mass measurement yields consistent results (within the sampling error) of $\sigma(\sigma_8) = 0.0046(0.0040)$. CMB-cluster lensing cluster mass measurements will be important to achieving the full potential of cluster cosmology over this decade.

6. Conclusions and Outlook

We present the first cosmological parameter constraints incorporating CMB-cluster lensing mass estimates from the South Pole Telescope. While the CMB-cluster lensing mass information does not yet substantively improve cosmological constraints as compared to B19, this work serves as a demonstration for the method, which will be important for the next generation of large galaxy cluster surveys.

We show that adding CMB-cluster lensing mass measurements should significantly improve cosmological constraints from ongoing cluster surveys such as SPT-3G. In the seven-parameter wCDM cosmological model, we find that adding CMB-cluster lensing mass estimates to cluster number counts leads to a factor of 1.3 reduction in the uncertainty of w and a factor of 2.4 on σ_8.

CMB-cluster lensing data remains significant for the larger galaxy cluster catalog expected for CMB-S4. For CMB-S4, we find that the CMB-cluster lensing data reduces the uncertainty on σ_8 by a factor of 3.6. CMB-cluster lensing has the potential to significantly expand the cosmological information we can extract from galaxy cluster surveys.

ORCID iDs

C. L. Reichardt ⓘ https://orcid.org/0000-0003-2226-9169
N. Gupta ⓘ https://orcid.org/0000-0001-7652-9451
E. J. Baxter ⓘ https://orcid.org/0000-0002-6836-3196
S. Bocquet ⓘ https://orcid.org/0000-0002-4900-805X
T. M. Crawford ⓘ https://orcid.org/0000-0001-9000-5013
M. A. Dobbs ⓘ https://orcid.org/0000-0001-7166-6422
W. B. Everett ⓘ https://orcid.org/0000-0002-5370-6651
B. Floyd ⓘ https://orcid.org/0000-0003-4175-571X
E. M. George ⓘ https://orcid.org/0000-0001-7874-0445
S. S. Meyer ⓘ https://orcid.org/0000-0003-3315-4332
L. M. Mocanu ⓘ https://orcid.org/0000-0002-2416-2552
F. Ruppin ⓘ https://orcid.org/0000-0002-0955-8954
A. A. Stark ⓘ https://orcid.org/0000-0002-2718-9996
J. D. Vieira ⓘ https://orcid.org/0000-0001-7192-3871

References

Allen, S. W., Evrard, A. E., & Mantz, A. B. 2011, ARA&A, 49, 409
Baxter, E. J., Keisler, R., Dodelson, S., et al. 2015, ApJ, 806, 247
Baxter, E. J., Raghunathan, S., Crawford, T. M., et al. 2018, MNRAS, 476, 2674
Benson, B. A., Ade, P. A. R., Ahmed, Z., et al. 2014, Proc. SPIE, 9153, 91531P
Bleem, L. E., Stalder, B., de Haan, T., et al. 2015, ApJS, 216, 27
Bocquet, S., Dietrich, J. P., Schrabback, T., et al. 2019, ApJ, 878, 55
Cash, W. 1979, ApJ, 228, 939
CMB-S4 Collaboration 2019, arXiv:1907.04473
de Haan, T., Benson, B. A., Bleem, L. E., et al. 2016, ApJ, 832, 95
Dietrich, J. P., Bocquet, S., Schrabback, T., et al. 2019, MNRAS, 483, 2871
Dodelson, S. 2004, PhRvD, 70, 023009
Euclid Collaboration, Adam, R., Vannier, M., et al. 2019, A&A, 627, A23
Feroz, F., Hobson, M., & Bridges, M. 2009, MNRAS, 398, 1601
Foreman-Mackey, D., Hogg, D. W., Lang, D., & Goodman, J. 2013, PASP, 125, 306
Grandis, S., Mohr, J. J., Dietrich, J. P., et al. 2019, MNRAS, 488, 2041
Gupta, N., & Reichardt, C. L. 2021, ApJ, 923, 96
Haiman, Z., Mohr, J. J., & Holder, G. P. 2001, ApJ, 553, 545
Holder, G. 2006, arXiv:astro-ph/0602251
Holder, G., & Kosowsky, A. 2004, ApJ, 616, 8
Hu, W., DeDeo, S., & Vale, C. 2007, NJPh, 9, 441
Hunter, J. D. 2007, CSE, 9, 90
Jones, E., Oliphant, T., Peterson, P., et al. 2001, SciPy: Open Source Scientific Tools for Python, http://www.scipy.org/
Lafayette, L., Sauter, G., Vu, L., & Meade, B. 2016, OpenStack Summit, Barcelona, doi:10.4225/49/58ead90dceaaa
Lewis, A., & Challinor, A. 2006, PhR, 429, 1
Lewis, A., Challinor, A., & Lasenby, A. 2000, ApJ, 538, 473
Lewis, A., & King, L. 2006, PhRvD, 73, 063006
LSST Science Collaboration, Abell, P. A., Allison, J., et al. 2009, arXiv:0912.0201
Madhavacheril, M., Sehgal, N., Allison, R., et al. 2015, PhRvL, 114, 151302
McClintock, T., Varga, T. N., Gruen, D., et al. 2019, MNRAS, 482, 1352
McDonald, M., Allen, S. W., Bayliss, M., et al. 2017, ApJ, 843, 28
McDonald, M., Benson, B. A., Vikhlinin, A., et al. 2013, ApJ, 774, 23
Melin, J.-B., & Bartlett, J. G. 2015, A&A, 578, A21
Merloni, A., Predehl, P., Becker, W., et al. 2012, arXiv:1209.3114
Navarro, J. F., Frenk, C. S., & White, S. D. M. 1997, ApJ, 490, 493
Planck Collaboration, Ade, P. A. R., Aghanim, N., et al. 2016, A&A, 594, A24
Planck Collaboration, Aghanim, N., Akrami, Y., et al. 2020, A&A, 641, A5
Raghunathan, S., Patil, S., Baxter, E., et al. 2019a, PhRvL, 123, 181301
Raghunathan, S., Patil, S., Baxter, E., et al. 2019b, ApJ, 872, 170
Raghunathan, S., Patil, S., Baxter, E. J., et al. 2017, JCAP, 8, 030
Reichardt, C. L., Stalder, B., Bleem, L. E., et al. 2013, ApJ, 763, 127
Salvati, L., Douspis, M., & Aghanim, N. 2018, A&A, 614, A13
Salvati, L., Douspis, M., Ritz, A., Aghanim, N., & Babul, A. 2019, A&A, 626, A27
Schrabback, T., Applegate, D., Dietrich, J. P., et al. 2018, MNRAS, 474, 2635
Seljak, U., & Zaldarriaga, M. 2000, ApJ, 538, 57
Shimon, M., Sadeh, S., & Rephaeli, Y. 2011, MNRAS, 412, 1895
Sobrin, J. A., Anderson, A. J., Bender, A. N., et al. 2022, ApJS, 258, 42
The LSST Dark Energy Science Collaboration, Mandelbaum, R., Eifler, T., et al. 2018, arXiv:1809.01669
To, C., Krause, E., Rozo, E., et al. 2021, PhRvL, 126, 141301
Vale, A., & Ostriker, J. P. 2004, MNRAS, 353, 189

van der Walt, S., Colbert, S., & Varoquaux, G. 2011, CSE, 13, 22
Vanderlinde, K., Crawford, T. M., de Haan, T., et al. 2010, ApJ, 722, 1180
Wang, L., & Steinhardt, P. J. 1998, ApJ, 508, 483
Weller, J., & Battye, R. A. 2003, NewAR, 47, 775
Weller, J., Battye, R. A., & Kneissl, R. 2002, PhRvL, 88, 231301

Zohren, H., Schrabback, T., van der Burg, R. F. J., et al. 2019, MNRAS, 488, 2523
Zubeldia, Í., & Challinor, A. 2019, MNRAS, 489, 401
Zubeldia, Í., & Challinor, A. 2020, MNRAS, 497, 5326
Zuntz, J., Paterno, M., Jennings, E., et al. 2015, A&C, 12, 45